We are IntechOpen, the world's leading publisher of Open Access books
Built by scientists, for scientists

6,900
Open access books available

186,000
International authors and editors

200M
Downloads

154
Countries delivered to

Our authors are among the

TOP 1%
most cited scientists

12.2%
Contributors from top 500 universities

CLARIVATE ANALYTICS
BOOK CITATION INDEX
INDEXED

WEB OF SCIENCE™

Selection of our books indexed in the Book Citation Index
in Web of Science™ Core Collection (BKCI)

Interested in publishing with us?
Contact book.department@intechopen.com

Chapter

Optimization of MEMS Actuator Driven by Shape Memory Alloy Thin Film Phase Change

Cory R. Knick

Abstract

At the microscale, shape memory alloy (SMA) microelectromechanical system (MEMS) bimorph actuators offer great potential based on their inherently high work density. An optimization problem relating to the deflection and curvature based on shape memory MEMS bimorph was identified, formulated, and solved. Thicknesses of the SU-8 photoresist and nickel-titanium alloy (NiTi) was identified that yielded maximum deflections and curvature radius based on a relationship among individual layer thicknesses, elastic modulus, and cantilever length. This model should serve as a guideline for optimal NiTi and SU-8 thicknesses to drive large deflections and curvature radius that are most suitable for microrobotic actuation, micromirrors, micropumps, and microgrippers. This model would also be extensible to other phase-change-driven actuators where nonlinear and significant residual stress changes are used to drive actuation.

Keywords: shape memory alloy, thin film, microactuators, MEMS, optimization, radius of curvature, phase change

1. Introduction

In certain applications for MEMS microactuators, large deflections would be desired such as the case of micro-robotics [1–3], micromirrors [4–6], and microgrippers [3, 7]. Using a shape memory alloy (SMA), a material that undergoes large changes in stress during a temperature cycle due to a solid-solid phase change can be used to generate large, nonlinear deflections. We aim to find a relationship between deflections of a SMA MEMS actuator, and maximize the deflection of SMA MEMS bimorph. Shape memory alloy films based on sputtered NiTi have been exhaustively characterized in previous decades, leading to a wealth of information about the intricate interplay between Ni/Ti ratio, annealing temperatures and times, and thickness [8–31]. Bimorphic actuators can impart reversible deflection shape memory microactuators as previously demonstrated [32, 33].

To date, optimization of parameters for improving shape memory-induced actuation has not been explored. We chose for our candidate system an SU-8 patterned on top of NiTi SMA bimorph actuator. In this case, residual strains develop during the processing of MEMS actuators, and upon release from substrate, the device curls upward to relieve these strains. Thermal input converts the material into austenite, and shape memory effect drives the actuator into a more flat

position, a process that is reversible upon subsequent thermal cycles. Thermal effects can be delivered to the SMA MEMS using laser irradiation [34], and joule-heating [35], at frequencies up to at least 1 kHz. SU-8 is an ideal material due to its relative ease of use in MEMS, low modulus of elasticity enables more flexible devices with large deflection, and good chemical stability.

Much literature exists for thin film development and characterization of nickel-titanium shape memory alloy [1–4]. Although many demonstrations of SMA MEMS actuators have been shown [9, 34–43], none of these citations perform design optimization studies to maximize deflection or curvature radius due to residual stress changes due to phase change. When the nitinol is thermally cycled between martensite and austenite phases, there is a corresponding change in residual stress, which is used to drive the nonlinear deflections. This nonlinear and large change in stress is defined as the recovery stress, and is a principal factor influencing the deflection and curvature radius. Our novel contributions take a realistic SMA MEMS bimorph design based on SU-8 on NiTi, and determine optimal thickness combinations to yield maximized deflections, which would be desirable in certain applications were large strokes are desired. We feed into the model the Young's modulus values for NiTi thin films that have been determined previously using nanoindentation techniques [44, 45].

2. Building and characterizing the SMA MEMS actuators

The nickel-titanium alloy (NiTi) would be co-sputtered onto a 4″ silicon wafer based on the methods reported in previous works [8, 34–36]. The substrate is rotated and heated during deposition to ensure crystallization of the film. The wafer stress vs. temperature measurements are performed, using Stoney's equation to determine recovery stress, hysteresis, and residual stress in the NiTi film. After verification of good shape memory alloy properties in the film at wafer level, a photomask is used to pattern bimorph actuator. Ion milling is used to remove portions of the NiTi film on the wafer. The SU-8 2000.5 is spin coated (where the RPM is used to control SU-8 thickness) and another mask plate is used to pattern SU-8 on top of the NiTi cantilever. Finally, the device is released by etching the Si substrate away in xenon difluoride (XeF2) gas. In practice, SU-8 thickness would be controlled by varying spin speed, and NiTi thickness based on sputtering time.

2.1 Problem identification

The design problem is to maximize the deflection of a MEMS bimorph cantilever beam based on the nonlinear shape memory alloy (SMA) as the actuating mechanism. The deflection is dependent in large part on the parameter called recovery stress. The larger the recovery stress, the larger the deflection. We may also wish to decrease the overall mass or volume of the actuator, of minimize the curvature radius. The objectives are competing in that reduction in the shape memory alloy thickness, generally leads to reduction of the recovery stress. The bimorph actuator could consist of SU-8 on top of NiTi thin film, but this optimization model would be easily extensible to other cases of interest.

We should consider that the equation describing the recovery stress-induced deflection in shape memory alloy MEMS actuator is (Eq. 1).

Initially, the contour plots of SU-8 and NiTi thickness showed that the optimization problem was not interesting for the simplest case of constant recovery stress over the range of NiTi thickness. To our advantage, the NiTi recovery stress is a parameter that depends on NiTi thickness, which makes the optimization problem

more interesting. The equation describing the recovery stress-induced deflection in shape memory alloy (SMA) MEMS actuator is:

$$d = \frac{3E_{NiTi}\sigma_{rec}t_{NiTi}t_{SU\text{-}8}(t_{NiTi} + t_{SU\text{-}8})l^2}{E_{NiTi}^2 t_{NiTi}^4 + E_{SU\text{-}8}E_{NiTi}\left(4t_{NiTi}^3 t_{SU\text{-}8} + 6t_{NiTi}^2 t_{SU\text{-}8}^2 + 4t_{NiTi}t_{SU\text{-}8}^3\right) + E_{SU\text{-}8}^2 t_{SU\text{-}8}^4} \quad (1)$$

where σ_{rec} = recovery stress of the SMA MEMS actuator; d = deflection of the SMA MEMS actuator; l = total length of the SMA MEMS actuator; E_{NiTi} = elastic modulus of NiTi layer; $E_{SU\text{-}8}$ = elastic modulus of SU-8 layer; T_{NiTi} = thickness modulus of NiTi layer; $T_{SU\text{-}8}$ = thickness modulus of SU-8 layer.

Figure 1 shows stress vs. temperature curves for NiTi on Si wafer. These curves are experimentally generated, and indicate the recovery stress (difference between highest and lowest stress values), and the thermal hysteresis. Here, as an illustrative example, the NiTi thickness is 900 nm, and the temperature cycle is performed using a heating and cooling rate of 1°C/min.

Assumptions: we assume operating temperatures go between RT and 100°C to ensure full phase change. In all calculations, for simplicity we use Young's modulus of NiTi as a fixed value. In reality, the Young's modulus changes curing the phase change. Martensite (lower temperature phase usually has a lower elastic modulus compared to the higher temperature austenite phase).

Figure 2 shows the process used to build the SMA MEMS bimorph actuator comprised of the NiTi shape memory (SMA) layer underneath the SU-8 elastic layer. In step (a) deposition of SMA onto Si wafer and pattern using photolithography. In step (b) ion milling is performed to transfer the pattern into the SMA layer. In step (c) we spin on SU-8 and pattern it with mask plate and photolithography. In step (d) we release the MEMS bimorph by etching Si substrate with xenon difluoride (XeF$_2$) gas. In step (e) we thermally actuate the two-way shape memory MEMS device between curled and flat states.
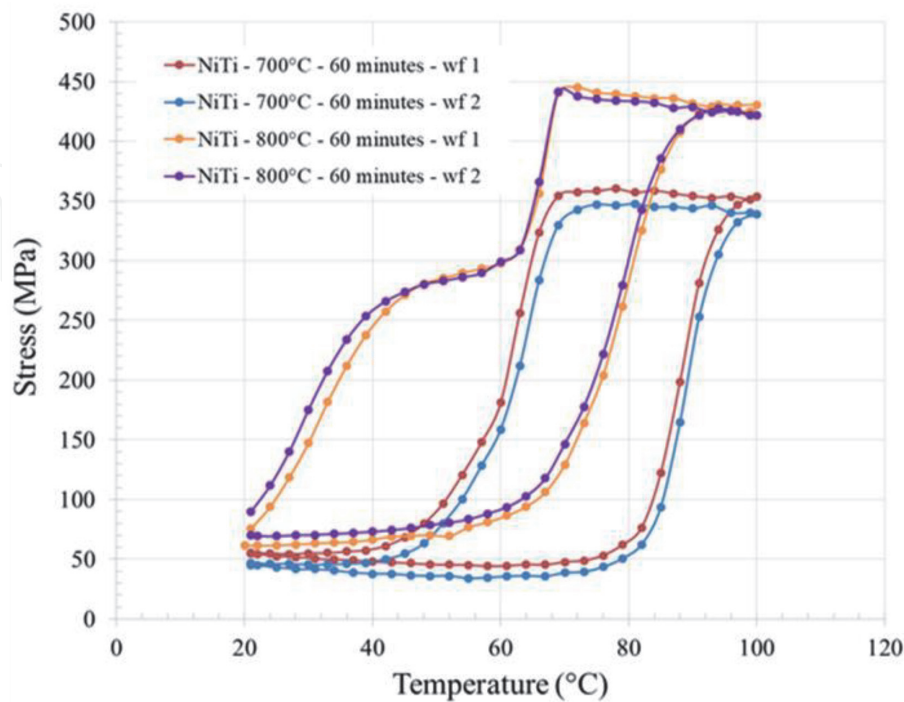

Figure 1.
Stress vs. temperature curves for NiTi on Si wafer. These curves are experimentally generated, and indicate the recovery stress (difference between highest and lowest stress values), and the thermal hysteresis.
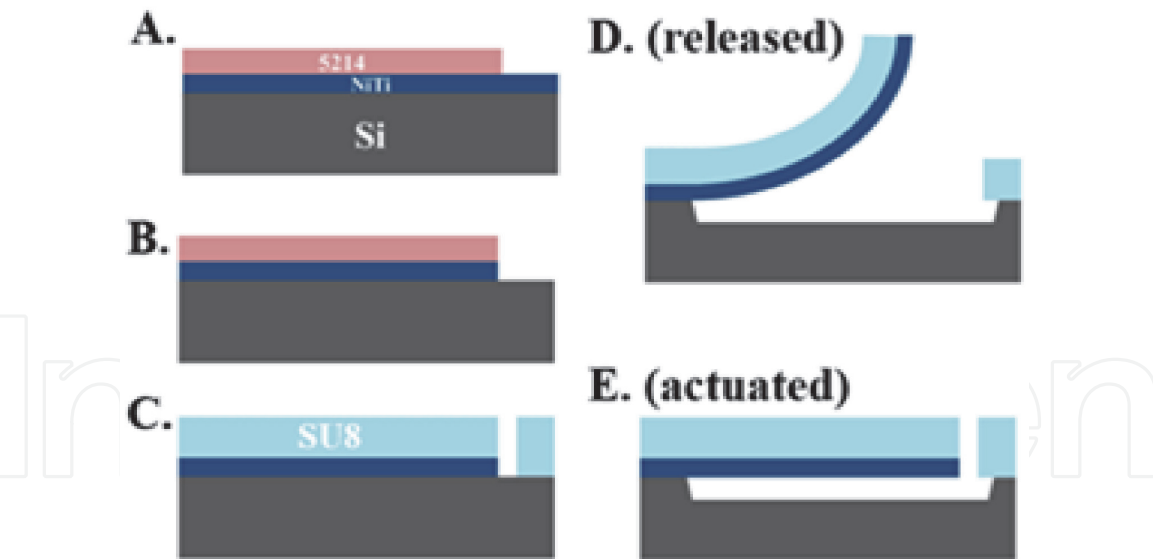
Figure 2.
SMA MEMS fabrication process for SU-8 on NiTi bimorph.

3. Methods, results, and discussions

3.1 Single-objective optimization

Regarding NiTi recovery stress, there would appear to be an optimal thickness range for which recovery stress reaches max values as depicted in **Figure 3**, below which there is a sharp drop off. Therefore the tendency for increased deflections for thinner materials reaches a point of diminishing returns due to the effect of decreasing recovery stress. Below 100–150 nm, shape memory properties have been
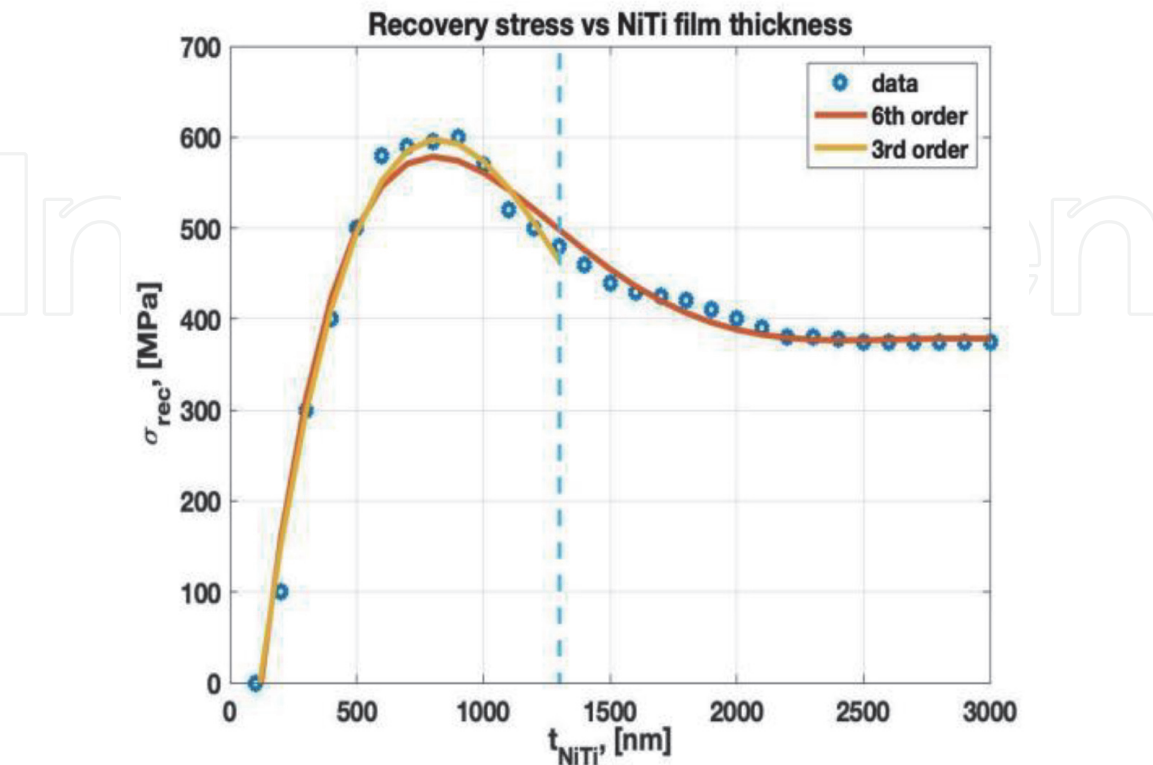

Figure 3.
Relation between recovery stress (MPa) and NiTi film thickness (nm).

shown to drop off completely, so we impose constraints for NiTi thickness to vary between 150 and 1300 nm.

Based on the curve fitting equation (*third-order polynomial*), the single-objective optimization problem can be written as following:

$$maximize :$$

$$d = \frac{3E_{NiTi}\sigma_{rec}t_{NiTi}t_{SU\text{-}8}(t_{NiTi} + t_{SU\text{-}8})l^2}{E_{NiTi}^2 t_{NiTi}^4 + E_{SU\text{-}8}E_{NiTi}\left(4t_{NiTi}^3 t_{SU\text{-}8} + 6t_{NiTi}^2 t_{SU\text{-}8}^2 + 4t_{NiTi}t_{SU\text{-}8}^3\right) + E_{SU\text{-}8}^2 t_{SU\text{-}8}^4} \quad (2)$$

subjected to::

$$100\ \mu m \le l \le 300\ \mu m \quad (3)$$

$$150\ nm \le t_{NiTi} \le 1000\ nm \quad (4)$$

$$200\ nm \le t_{SU\text{-}8} \le 2000\ nm \quad (5)$$

$$\sigma_{rec} \ge 0 \quad (6)$$

$$\sigma_{rec} = 5.36E26t_{NiTi}{}^3 - 2.15E21t_{NiTi}{}^2 + 2.45E15t_{NiTi} - 2.58E08\ \text{(SI units)} \quad (7)$$

Covert to standard form in SI units:

$$minimize :$$

$$f = \frac{-3E_{NiTi}\sigma_{rec}t_{NiTi}t_{SU\text{-}8}(t_{NiTi} + t_{SU\text{-}8})l^2}{E_{NiTi}^2 t_{NiTi}^4 + E_{SU\text{-}8}E_{NiTi}\left(4t_{NiTi}^3 t_{SU\text{-}8} + 6t_{NiTi}^2 t_{SU\text{-}8}^2 + 4t_{NiTi}t_{SU\text{-}8}^3\right) + E_{SU\text{-}8}^2 t_{SU\text{-}8}^4} \quad (8)$$

subjected to::

$$g_1 : 100 \times 10^{-6} - l \le 0; \quad (9)$$

$$g_2 : l - 300 \times 10^{-6} \le 0; \quad (10)$$

$$g_3 : 150 \times 10^{-9} - t_{NiTi} \le 0; \quad (11)$$

$$g_4 : t_{NiTi} - 1300 \times 10^{-9} \le 0; \quad (12)$$

$$g_5 : 200 \times 10^{-9} - t_{SU\text{-}8} \le 0; \quad (13)$$

$$g_6 : t_{SU\text{-}8} - 2000 \times 10^{-9} \le 0; \quad (14)$$

$$g_7 : -\sigma_{rec} \le 0 \quad (15)$$

$$h_1 : \sigma_{rec} - 5.36 \times 10^{26}t_{NiTi}{}^3 + 2.15 \times 10^{21}t_{NiTi}{}^2 - 2.45 \times 10^{15}t_{NiTi} + 2.58 \times 10^8 = 0 \quad (16)$$

3.2 MATLAB optimization toolbox (fmincon)

According to the toolbox (and as shown in **Figure 4**), optimal solution is: $t_{NiTi} = 359\ nm, t_{SU\text{-}8} = 824\ nm, l = 300\ \mu m$.

3.3 Multi-objective optimization

The curvature of a bilayer elastic material [46] is given as

$$K = \frac{-E'_{SU\text{-}8}t_{SU\text{-}8}E'_{NiTi}t_{NiTi}(t_{NiTi} + t_{SU\text{-}8})}{G\left(E'_{SU\text{-}8}t_{SU\text{-}8} + E'_{NiTi}t_{NiTi}\right)}\Delta\varepsilon \quad (17)$$
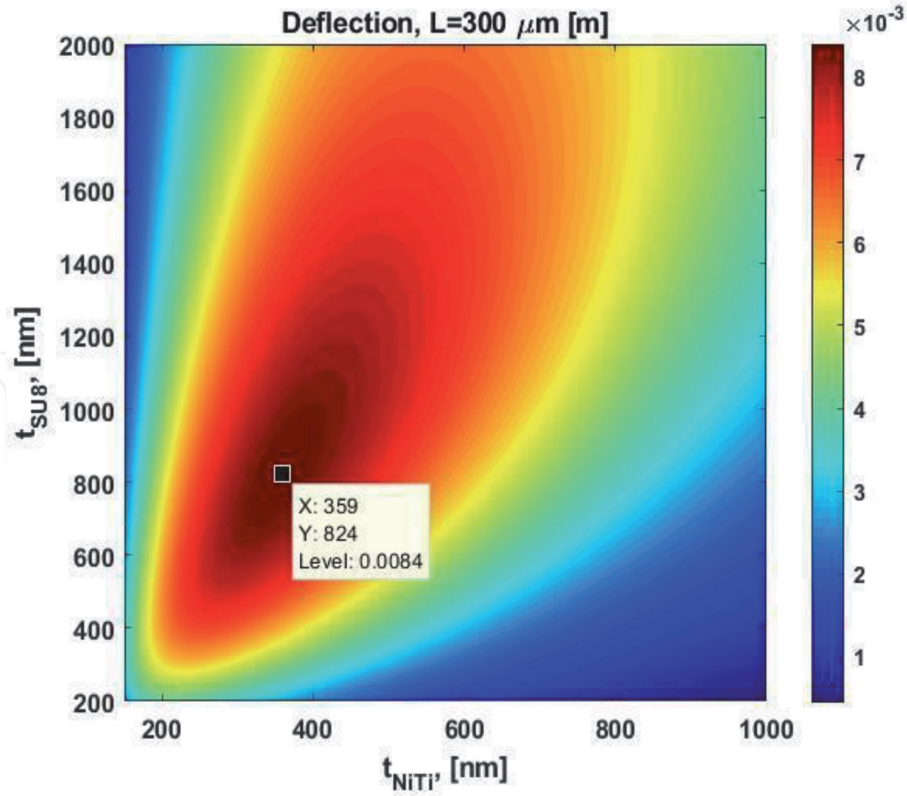
Figure 4.
Optimization contours for the case where SU-8 elastic modulus is 2 GPa. Variables considered are individual layer thicknesses: NiTi (x-axis) and SU-8 (y-axis).

$$G = E'_{SU-8}t^2_{SU-8}\left(\frac{t_{NiTi}}{2} - \frac{t_{SU-8}}{6} - \theta\right) - E'_{NiTi}t_{NiTi}\left[t_{SU-8}\left(t_{SU-8} + \frac{t_{NiTi}}{2}\right) + \frac{t^2_{NiTi}}{6} + \theta(2t_{SU-8} + t_{NiTi})\right] \quad (18)$$

$$\theta = \frac{t_{NiTi}t_{SU-8}\left(E'_{NiTi} - E'_{SU-8}\right)}{2\left(E'_{SU-8}t_{SU-8} + E'_{NiTi}t_{NiTi}\right)} \quad (19)$$

$$\Delta\varepsilon = (\alpha_{SU-8} - \alpha_{NiTi})\Delta T \quad (20)$$

ρ is the curvature radius generally expressed in units of μm. $\Delta\varepsilon$ is a strain differential term resulting from CTE mismatch and temperature difference experienced during the processing. θ is a correction factor used in the placement of neutral plane. E' is the biaxial modulus defined as $E/(1-v)$ where v is Poisson ratio and E is Young's modulus. Poisson ratios are assumed to be 0.22 for SU-8 and 0.33 for NiTi. α_SU-8 is reported to be 52×10^{-6}/°C. α_NiTi (depending on austenite or martensite phase) is reported to be 6.6 or 11×10^{-6}/°C. For simplicity sake, we assume an intermediate value of $\alpha\_NiTi = 9 \times 10^{-6}$/°C. Units for theta term is nm or m. Units for G term is Pa × nm³ or Pa × m³. Therefore units for curvature is in nm or m. $\Delta\varepsilon$ term is unit less.

The objective number 2 is to maximize curvature radius. We determine the pareto frontier and strong pareto points using the epsilon constrained method. In this epsilon constrained method, we minimize f1 while keeping f2 less than or equal to different values of epsilon. As a first step for objective function 2 (curvature of bimorph) we coded MATLAB script to generate contour plots as a function of the two main design variables (i.e., thickness of NiTi and SU-8). The problem formulation for objective function 2 is as follows (and contour plot is shown in **Figure 5**).

Curvature is:

$$K = -\frac{E'_{SU-8}t_{SU-8}E'_{NiTi}t_{NiTi}(t_{NiTi} + t_{SU-8})}{G\left(E'_{SU-8}t_{SU-8} + E'_{NiTi}t_{NiTi}\right)}\Delta\varepsilon \quad (21)$$

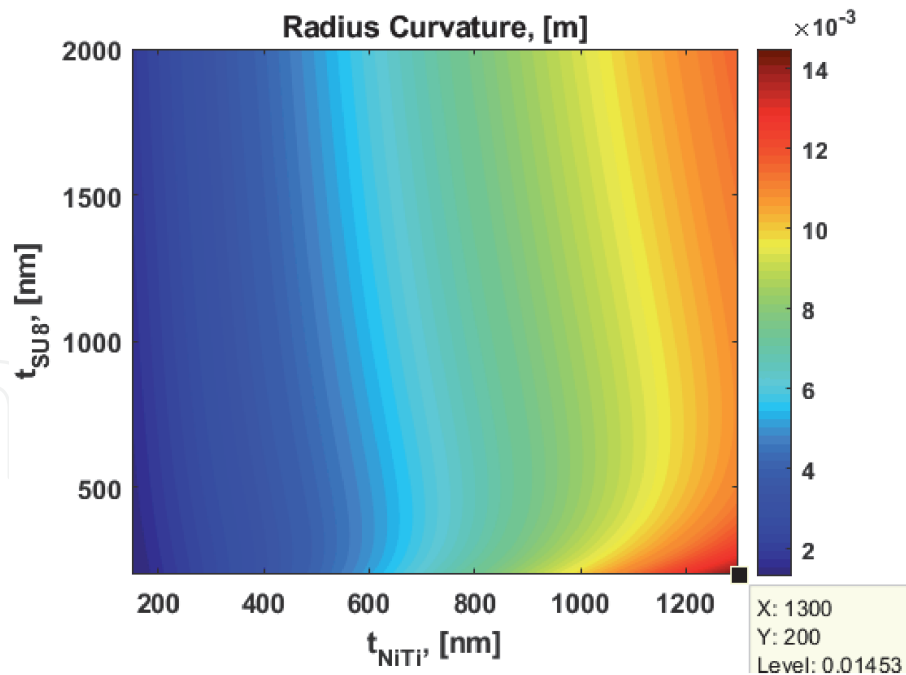**Figure 5.**
MATLAB-generated contour plot of curvature radius (m), against the primary design variables (i.e., tNiTi and t_{SU-8}). Curvature radius is maximized for the thickest values of NiTi and thinnest values of SU-8. The result is intuitive because this is the stiffest beam (from the perspective of thickest NiTi with much larger Young's modulus compared to SU-8). Thinner SU-8 means the effect from strain differential and CTE mismatch is minimized and contributes less to curvature radius. Overall, this means that upper bound on NiTi thickness and lower bound on SU-8 thickness are active constraints for objective function 2.

Maximize:

$$\rho = \frac{1}{K} = -\frac{G\left(E'_{SU\text{-}8}t_{SU\text{-}8} + E'_{NiTi}t_{NiTi}\right)}{E'_{SU\text{-}8}t_{SU\text{-}8}E'_{NiTi}t_{NiTi}(t_{NiTi} + t_{SU\text{-}8})\Delta\varepsilon} \tag{22}$$

Subjected to:

$$g_1 : 150 \times 10^{-9} - t_{NiTi} \leq 0; \tag{23}$$

$$g_2 : t_{NiTi} - 1300 \times 10^{-9} \leq 0; \tag{24}$$

$$g_3 : 200 \times 10^{-9} - t_{SU\text{-}8} \leq 0; \tag{25}$$

$$g_4 : t_{SU\text{-}8} - 2000 \times 10^{-9} \leq 0; \tag{26}$$

$$h_1 : G - E'_{SU\text{-}8}t^2_{SU\text{-}8}\left(\frac{t_{NiTi}}{2} - \frac{t_{SU\text{-}8}}{6} - \theta\right)$$
$$- E'_{NiTi}t_{NiTi}\left[t_{SU\text{-}8}\left(t_{SU\text{-}8} + \frac{t_{NiTi}}{2}\right) + \frac{t^2_{NiTi}}{6} + \theta(2t_{SU\text{-}8} + t_{NiTi})\right]$$
$$= 0 \tag{27}$$

$$h_2 : \theta - \frac{t_{NiTi}t_{SU\text{-}8}\left(E'_{NiTi} - E'_{SU\text{-}8}\right)}{2\left(E'_{SU\text{-}8}t_{SU\text{-}8} + E'_{NiTi}t_{NiTi}\right)} = 0 \tag{28}$$

For multi-objective optimization, the deflection and curvature radius of *SMA* bimorph actuator are maximized simultaneously. So, the multi-objective optimization problem can be stated as follows:

maximize:

$$f_1 : \rho = -\frac{G\left(E'_{SU\text{-}8}t_{SU\text{-}8} + E'_{NiTi}t_{NiTi}\right)}{E'_{SU\text{-}8}t_{SU\text{-}8}E'_{NiTi}t_{NiTi}(t_{NiTi} + t_{SU\text{-}8})\Delta\varepsilon} \tag{29}$$

$$f_2 : d = \frac{3E_{NiTi}\sigma_{rec}t_{NiTi}t_{SU\text{-}8}(t_{NiTi} + t_{SU\text{-}8})l^2}{E_{NiTi}^2 t_{NiTi}^4 + E_{SU\text{-}8}E_{NiTi}\left(4t_{NiTi}^3 t_{SU\text{-}8} + 6t_{NiTi}^2 t_{SU\text{-}8}^2 + 4t_{NiTi}t_{SU\text{-}8}^3\right) + E_{SU\text{-}8}^2 t_{SU\text{-}8}^4}$$

(30)

Subjected to:

$$g_1 : 100 \times 10^{-6} - l \leq 0; \tag{31}$$

$$g_2 : l - 300 \times 10^{-6} \leq 0; \tag{32}$$

$$g_3 : 150 \times 10^{-9} - t_{NiTi} \leq 0; \tag{33}$$

$$g_4 : t_{NiTi} - 1300 \times 10^{-9} \leq 0; \tag{34}$$

$$g_5 : 200 \times 10^{-9} - t_{SU\text{-}8} \leq 0; \tag{35}$$

$$g_6 : t_{SU\text{-}8} - 2000 \times 10^{-9} \leq 0; \tag{36}$$

$$g_7 : -\sigma_{rec} \leq 0; \tag{37}$$

$$h_1 : \sigma_{rec} - 5.36 \times 10^{26}t_{NiTi}^3 + 2.15 \times 10^{21}t_{NiTi}^2 - 2.45 \times 10^{15}t_{NiTi} + 2.58 \times 10^8 = 0; \tag{38}$$

$$h_2 : G - E'_{SU\text{-}8}t_{SU\text{-}8}^2\left(\frac{t_{NiTi}}{2} - \frac{t_{SU\text{-}8}}{6} - \theta\right) - E'_{NiTi}t_{NiTi}\left[t_{SU\text{-}8}\left(t_{SU\text{-}8} + \frac{t_{NiTi}}{2}\right) + \frac{t_{NiTi}^2}{6} + \theta(2t_{SU\text{-}8} + t_{NiTi})\right] = 0; \tag{39}$$

$$h_3 : \theta - \frac{t_{NiTi}t_{SU\text{-}8}\left(E'_{NiTi} - E'_{SU\text{-}8}\right)}{2\left(E'_{SU\text{-}8}t_{SU\text{-}8} + E'_{NiTi}t_{NiTi}\right)} = 0. \tag{40}$$

Due to the conflicting nature of the two objective functions, the contour plot for the multi-objective function has changed substantially. Maximizing the radius is favored by a larger t_{NiTi} as opposed to a smaller thickness required to maximize
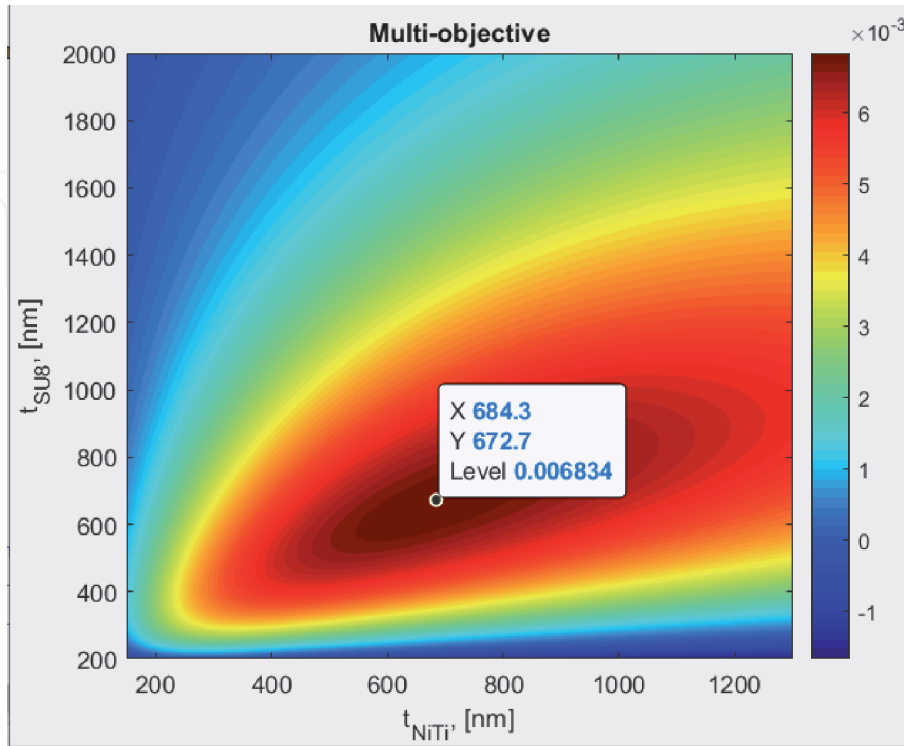

Figure 6.
Optimal solution for simultaneous multi-objective optimization of deflection and curvature radius.
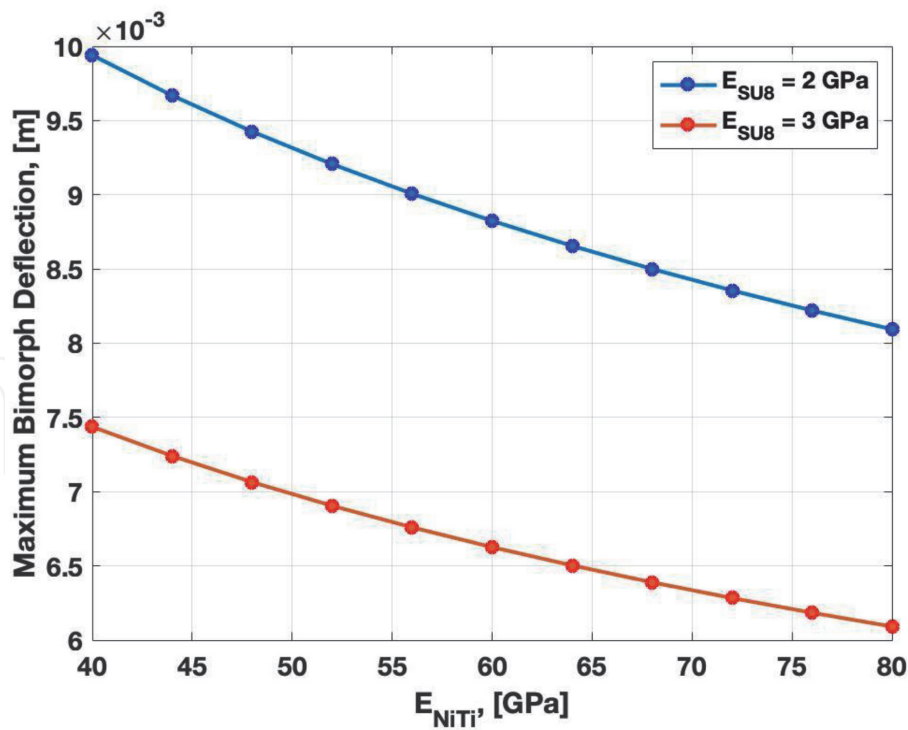
Figure 7.
Maximum bimorph deflection with a variation of Young's modulus of NiTi and SU-8 layer.

deflection. The optimal solution of multi-objective function as shown in **Figure 6** has a larger t_{NiTi}.

Once we have established the optimal objective values for deflection and curvature, we perform a sensitivity analysis regarding the following variables, for which experimentally could be varied with relative ease. These thickness values x1 and x2, corresponding the NiTi and SU-8 thicknesses, can be changed by varying the spin speed for SU-8 coating: faster spins corresponding to thinner films of SU-8 and vice versa. For NiTi, longer sputter time would be used for thicker films and vice versa. Young's modulus can be varied by deposition conditions for NiTi and curing/baking temperatures and conditions for SU-8. To perform the sensitivity analysis for Objective 1, we keep fixed the optimal thickness for SU-8 and vary the NiTi thickness to see how it changes, and plot a function (as shown in **Figure** 7) and generate a table of values. Similarly, we keep fixed the optimal value of NiTi thickness and recovery stress, and plot the deflection over a range of SU-8 thicknesses.

4. Conclusions

In conclusion, an interesting optimization problem was identified whereby the deflection of shape memory MEMS bimorph actuator was maximized. Original calculations showed that reductions in the thickness of the bimorph layers would yield maximized deflections (for the simplest case assuming constant values of recovery stress in NiTi layer). In the literature, a more complex relationship among recovery stress and the NiTi thickness was identified. A curve fit to this data yielded a much more interesting optimization problem, which was solved graphically (contour plots) and using the Optimization Toolbox in MATLAB. Optimal NiTi and SU-8 thickness were determined to be for the case where SU-8 modulus was 2 GPa to be t_{NiTi} = 359 nm, t_{SU-8} = 824 nm. After solving the single-objective optimization problem using fmincon, Excel solver, and a hand-coded algorithm, we formulated a second objective function to maximize curvature radius (i.e., to maximize the

flatness of the beam because larger curvature radius is a flatter beam). We used fmincon to solve for the optimal values of NiTi and SU-8 to maximize the curvature radius. We determined that the objective functions were conflicting (i.e., there was clearly a tradeoff in order to satisfy both conditions simultaneously), and therefore suitable for multi-objective optimization. We formulated a multi-objective optimization method and solved it using fmincon. Finally, a parametric study or sensitivity analysis was performed pertaining to NiTi and SU-8 Young's modulus.

Acronyms and abbreviations

α_{NiTi}	CTE of NiTi layer
$\alpha_{SU\text{-}8}$	CTE of SU-8 layer
Bimorph	composite cantilever beam consisting of two materials with different Young's modulus and thickness
CTE	coefficient of thermal expansion
d	deflection of the *SMA MEMS* actuator (micrometer)
E_{NiTi}	elastic modulus of *NiTi* layer (GPa)
$E_{SU\text{-}8}$	elastic modulus of *SU-8* layer (GPa)
E'_{NiTi}	biaxial elastic modulus of *NiTi* layer (GPa)
$E'_{SU\text{-}8}$	biaxial elastic modulus of *SU-8* layer (GPa)
$\Delta\varepsilon$	strain differential arising from thermal processing and CTE mismatch
l	total length of the *SMA MEMS* actuator (micrometer)
MEMS	microelectromechanical system
ρ	curvature radius
σ_{rec}	recovery stress of the *SMA MEMS* actuator (MPa)
SMA	shape memory alloy (i.e., NiTi)
T_{NiTi}	thickness modulus of *NiTi* layer (nm)
$T_{SU\text{-}8}$	thickness modulus of *SU-8* layer (nm)
θ	correction factor term for location of neutral axis

Author details

Cory R. Knick
US Army Night Vision and Electronic Sensors Directorate, Ft. Belvoir, VA, USA

*Address all correspondence to: cory.r.knick.civ@mail.mil

IntechOpen

References

[1] Lee HT, Kim MS, Lee GY, Kim CS, Ahn SH. Shape memory alloy (SMA)-based microscale actuators with 60% deformation rate and 1.6 kHz actuation speed. Small. 2018;**14**:e1801023

[2] Liu K, Cheng C, Cheng Z, Wang K, Ramesh R, Wu J. Giant-amplitude, high-work density microactuators with phase transition activated nanolayer bimorphs. Nano Letters. 2012;**12**: 6302-6308

[3] Leong TG, Randall CL, Benson BR, Bassik N, Stern GM, Gracias DH. Tetherless thermobiochemically actuated microgrippers. Proceedings of the National Academy of Sciences of the United States of America. 2009;**106**: 703-708

[4] Ohnishi T, Sugimura A. Optical actuation of micromirrors fabricated by the micro-origami technique. Applied Physics Letters. 2009;**83**

[5] Ritt G, Eberle B. Automatic laser glare suppression in electro-optical sensors. Sensors (Basel). 2015;**15**: 792-802

[6] Murrer JRL, Goodwin SH, Dausch DE, Solomon SL, Lamvik MK. Electrostatic artificial eyelid actuator as an analog micromirror device. In: Proceedings SPIE 5785, Technologies for Synthetic Environments: Hardware-in-the-Loop Testing. Vol. 5785. 2005. p. 59

[7] Malachowski K, Jamal M, Jin Q, Polat B, Morris CJ, Gracias DH. Self-folding single cell grippers. Nano Letters. 2014;**14**:4164-4170

[8] Ainslie K, Knick C, Smith G, Li J, Troxel C, Mehta A, et al. Controlling shape memory effects in NiTi thin films grown on Ru seed layer. Sensors and Actuators A: Physical. 2019;**294**:133-139

[9] Choudhary N, Kaur D. Shape memory alloy thin films and heterostructures for MEMS applications: A review. Sensors and Actuators A: Physical. 2016;**242**:162-181

[10] Kotnur VG, Tichelaar FD, Fu WT, De Hosson JTM, Janssen GCAM. Shape memory NiTi thin films deposited on polyimide at low temperature. Surface and Coatings Technology. 2014;**258**: 1145-1151

[11] Sanjabi S, Sadrnezhaad SK, Barber ZH. Sputter alloying of Ni, Ti and Hf for fabrication of high temperature shape memory thin films. Materials Science and Technology. 2013; **23**:987-991

[12] Koker MKA, Schaab J, Zotov N, Mittemeijer EJ. X-ray diffraction study of the reverse martensitic transformation in NiTi shape memory thin films. Thin Solid Films. 2013;**545**: 71-80

[13] König D, Buenconsejo PJS, Grochla D, Hamann S, Pfetzing-Micklich J, Ludwig A. Thickness-dependence of the B2–B19 martensitic transformation in nanoscale shape memory alloy thin films: Zero-hysteresis in 75 nm thick Ti51Ni38Cu11 thin films. Acta Materialia. 2012;**60**:306-313

[14] Chung CY, Chan PM. NiTi shape memory alloy thin film micro-cantilevers array. Thin Solid Films. 2011;**519**:5307-5309

[15] Annadurai A, Manivel Raja M, Prabahar K, Kumar A, Kannan MD, Jayakumar S. Stress analysis, structure and magnetic properties of sputter deposited Ni–Mn–Ga ferromagnetic shape memory thin films. Journal of Magnetism and Magnetic Materials. 2011;**323**:2797-2801

[16] Satoh G, Birnbaum A, Yao YL. Annealing effect on the shape memory

properties of amorphous NiTi thin films. Journal of Manufacturing Science and Engineering. 2010;**132**:051004

[17] Rao J, Roberts T, Lawson K, Nicholls J. Nickel titanium and nickel titanium hafnium shape memory alloy thin films. Surface and Coatings Technology. 2010;**204**:2331-2336

[18] Ounaies Z, Mandepudi SK, Li J, Ackler HD. Processing and characterization of composite shape memory alloy (SMA) thin film structures for microactuators. Behavior and Mechanics of Multifunctional Materials and Composites. 2010;**7644**: 76440N

[19] Martins RMS, Schell N, Reuther H, Pereira L, Mahesh KK, Silva RJC, et al. Texture development, microstructure and phase transformation characteristics of sputtered Ni–Ti shape memory alloy films grown on TiN< 111>. Thin Solid Films. 2010;**519**: 122-128

[20] Sanjabi S, Barber ZH. The effect of film composition on the structure and mechanical properties of NiTi shape memory thin films. Surface and Coatings Technology. 2010;**204**: 1299-1304

[21] Wang X. Crystallization and martensitic transformation behavior of NiTi shape memory alloy thin films [PhD thesis]. Harvard: School of Engineering and Applied Sciences; 2007

[22] Wibowo E, Kwok CY. Fabrication and characterization of sputtered NiTi shape memory thin films. Journal of Micromechanics and Microengineering. 2006;**16**:101-108

[23] Fu YQ, Zhang S, Wu MJ, Huang WM, Du HJ, Luo JK, et al. On the lower thickness boundary of sputtered TiNi films for shape memory application. Thin Solid Films. 2006;**515**: 80-86

[24] Tomozawa M, Kim HY, Miyazaki S. Microactuators using R-phase transformation of sputter-deposited Ti-47.3Ni shape memory Alloy thin films. Journal of Intelligent Material Systems and Structures. 2006;**17**:1049-1058

[25] Getchel DJ, Savage RN. Fabrication and composition control of NiTi sape memory thin films for microactuators. Materials Research Society Symposium Proceedings. 2005;**875**:O6.4.1-O6.4.3

[26] Ishida A, Sato M, Tabata O, Yoshikawa W. Shape memory thin films formed with carrousel-type magnetron sputtering apparatus. Smart Materials and Structures. 2005;**14**:S216-S222

[27] Liu YS, Xu D, Jiang BH, Yuan ZY, Houtte PV. The effect of crystallizing procedure on microstructure and characteristics of sputter-deposited TiNi shape memory thin films. Journal of Micromechanics and Microengineering. 2005;**15**:575-579

[28] Ho KK, Carman GP, Jardine PA. Bimorphic, cmpositionally graded, sputter-deposited. Thin Film Shape Memory Alloys. 2004. US 6,689,586 B2

[29] Tingbin Wu BJ, Qi X, Liu Y, Xu D, Wang L. Residual stress of TiNi shape memory alloy thin films with (111) single-crystal silicon wafer. Materials Transactions. 2002;**43**:566-570

[30] Zohar Y, Wong M, Wang RX. Residual stress-loaded titanium–nickel shape memory alloy thin-film micro-actuators. Journal of Micromechanics and Microengineering. 2002;**12**:323-327

[31] Lehnert T, Crevoiserat S, Gotthardt R. Transformation properties and microstructure of sputter-deposited Ni-Ti shape memory alloy thin films. Journal of Materials Science. 2002;**37**

[32] Xiaobo Zhang YW, Miao X, Zhang C, Ding G. An electro-thermal SU-8 cantilever micro actuator based on

bimorph effect. In: Proceedings of the 2010 5th IEEE International Conference on Nano/Micro Engineered and Molecular Systems. Xiamen, China: IEEE; 2010. pp. 362-365

[33] Roch I, Bidaud P, Collard D, Buchaillot L. Fabrication and characterization of an SU-8 gripper actuated by a shape memory alloy thin film. Journal of Micromechanics and Microengineering. 2003;**13**:330-336

[34] Knick CR, Smith GL, Morris CJ, Bruck HA. Rapid and low power laser actuation of sputter-deposited NiTi shape memory alloy (SMA) MEMS thermal bimorph actuators. Sensors and Actuators A: Physical. 2019;**291**:48-57

[35] Knick CR, Sharar DJ, Wilson AA, Smith GL, Morris CJ, Bruck HA. High frequency, low power, electrically actuated shape memory alloy MEMS bimorph thermal actuators. Journal of Micromechanics and Microengineering. 2019;**29**:075005

[36] Knick CR, Morris CJ, Smith GL. Rapid and low power laser actuation of sputter-deposited NiTi shape memory alloy (SMA) MEMS thermal bimorph actuators. Sensors and Actuators A: Physical. 2019;**291**:48-57

[37] Mukesh Kumar S, Lakshmi MV. Applications of shape memory alloys in MEMS devices. International Journal of Advanced Research in Computer and Communication Engineering. 2013;**2**: 1122-1127

[38] Dahmardeh M, Mohamed Ali MS, Saleh T, Hian TM, Moghaddam MV, Nojeh A, et al. High-power MEMS switch enabled by carbon-nanotube contact and shape memory-alloy actuator. Physica Status Solidi. 2013; **210**:631-638

[39] Namazu T, Tashiro Y, Inoue S. Ti–Ni shape memory alloy film-actuated microstructures for a MEMS probe card.

Journal of Micromechanics and Microengineering. 2007;**17**:154-162

[40] Grummon DS, Gotthardt R, LaGrange T. Planar extrinsic biasing of thin film shape memory MEMS actuators. MRS Online Proceedings Library Archive. 2003;**741**:287-292

[41] Bergmann NW, Xu D, Cai B, Ding G, Zhou Y, Yu A, et al. Novel micropump actuated by thin film shape memory alloy. In: Electronics and Structures for MEMS. Queensland, Austrailia: SPIE; 1999. pp. 369-375

[42] Wolf RH, Heuer AH. TiNi (shape memory) films on Si for MEMS applications. Journal of Microelectromechanical Systems. 1995; **4**:206

[43] Fallon P. Gerratt A. Kierstead B, Robert W. Shape memory alloy and elastomer composite MEMS actuators. Technical Proceedings of 2008 NSTI Nanotechnology Conference and Tradeshow. Vol. 3. 2008

[44] Cole DP, Jin H, Lu W-Y, Roytburd AL, Bruck HA. Reversible nanoscale deformation in compositionally graded shape memory alloy films. Applied Physics Letters. 2009;**94**:193114

[45] Cole DP, Bruck HA, Roytburd AL. Nanoindentation studies of graded shape memory alloy thin films processed using diffusion modification. Journal of Applied Physics. 2008;**103**: 064315

[46] Klein CA, Miller RP. Strains and stresses in multilayered elastic structures: The case of chemically vapor-deposited ZnS/ZnSe laminates. Journal of Applied Physics. 2000;**87**(5): 2265-2272